Thermal Stability in Bulk Cryomilled Ultrafine-Grained 5083 Al Alloy

INDRANIL ROY, MANISH CHAUHAN, ENRIQUE J. LAVERNIA, and FARGHALLI A. MOHAMED

Thermal stability in bulk ultrafine-grained (UFG) 5083 Al that was processed by gas atomization followed by cryomilling, consolidation, and extrusion, and that exhibited an average grain size of 305 nm, was investigated in the temperature range of 473 to 673 K (0.55 to 0.79 T_m, where T_m is the melting temperature of the material) for different annealing times. Appreciable grain growth was observed at temperatures >573 K, whereas there was limited grain growth at temperatures <573 K even after long annealing times. The values of the grain growth exponent, n, deduced from the grain growth data were higher than the value of 2 predicted from elementary grain growth theories. The discrepancy was attributed to the operation of strong pinning forces on boundaries during the annealing treatment. An examination of the microstructure of the alloy suggests that the origin of the pinning forces is most likely related to the presence of dispersion particles, which are mostly introduced during cryomilling. Two-grain growth regimes were identified: the low-temperature region (<573 K) and the high-temperature region (>573 K). For temperatures lower than 573 K, the activation energy of 25 ± 5 kJ/mol was determined. It is suggested that this low activation energy represents the energy for the reordering of grain boundaries in the UFG material. For temperatures higher than 573 K, an activation energy of 124 ± 5 kJ/mol was measured. This value of activation energy, 124 ± 5 kJ/mol, lies between that for grain boundary diffusion and lattice diffusion in analogous aluminum polycrystalline systems. The results show that the strength and ductility of bulk UFG 5083 Al, as obtained from tensile tests, correlate well with substructural changes introduced in the alloy by the annealing treatment.

I. INTRODUCTION

NEAR nanostructured or ultrafine-grained (UFG) materials are defined as materials having grain sizes whose linear dimensions are in the range of 100 to 500 nm. The physical properties of these materials are potentially superior to those of their coarse-grained counterparts.[1–4] This potential superiority results from the reduced size or dimensionality of the near nanometer-sized crystallites as well as from the numerous interfaces between adjacent crystallites.[3] In this article, experimental data obtained on the thermal stability of the bulk UFG 5083 Al alloy and its strength at high temperatures are reported and analyzed. The alloy was processed by gas atomization followed by cryomilling, consolidation, hot isostatic pressing (hipping), and extrusion. The investigation was motivated by several considerations as described herein.

First, the properties associated with UFG alloys are closely related to the extremely fine grain size and the large volume fraction of grain boundaries. As a result, it is important to study the thermal stability of UFG alloys such as UFG 5083 Al for the purpose of identifying various factors that can contribute to maintaining the grain size at the ultrafine scale during high-temperature applications. Second, UFG alloys exhibit grain sizes that fall between the macro (>1 μm) and the nano (<100 nm) ranges. Accordingly, studying UFG alloys such as UFG 5083 Al can provide guiding information regarding the thermal stability of material systems in the transition region between these two ranges. Third, previous research focused on studying thermal stability and microstructures of cryomilled (milled under liquid nitrogen temperature) UFG alloys in different material systems in the *powder* form.[5–8] However, for structural applications, such studies need to be conducted on materials in the *bulk* form. At present, there are no data regarding thermal stability of UFG 5083 Al alloy in the bulk form. Finally, in order to study UFG 5083 Al alloy in the bulk form, the alloy was prepared by gas atomization followed by cryomilling, consolidation, and extrusion. The preparation of the bulk alloy using this procedure leads to introducing several substructural features including (a) oxide particles resulting from the breakup of oxide layers that are formed around metal particles during gas atomization, and (b) carbides, nitrides, and other impurities during cryomilling. Accordingly, an investigation of thermal stability of UFG 5083 Al alloy prepared by gas atomization followed by cryomilling, consolidation (hipping), and extrusion can provide information that may lead to the identification of the role played by the aforementioned substructural features regarding grain growth mechanisms and high-temperature strength.

II. EXPERIMENTAL PROCEDURE

A. *Material*

The target material, UFG 5083 Al, was selected for two main reasons. First, UFG 5083 Al alloy is a potential candidate for structural applications in aerospace and automobile industries. Second, data on the thermal stability of the alloy in the powder form are available. Accordingly, it is possible

INDRANIL ROY and MANISH CHAUHAN, Graduate Research Assistants, and FARGHALLI A. MOHAMED, Professor, are with the Department of Chemical Engineering and Materials Science, University of California, Irvine, CA 92697. Contact e-mail: famohame@uci.edu ENRIQUE J. LAVERNIA, Professor, is with the Department of Chemical Engineering and Materials Science, University of California, Davis, CA 95616.

Manuscript submitted May 25, 2005.

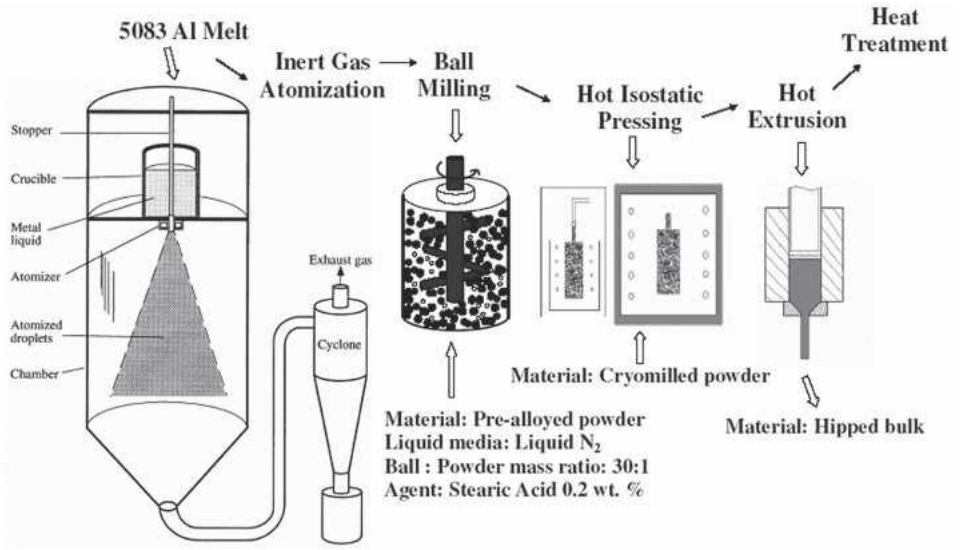

Fig. 1—Processing steps to produce bulk cryomilled UFG 5083 Al alloy.

to provide a direct comparison between the characteristics of the thermal stability of alloy in the bulk form and those reported for the alloy in the powder form.

B. *Processing*

5083 Al (4.4Mg, 0.7Mn, 0.15Cr, balance Al) was spray atomized.[9] The spray-atomized powder with a particle size less than 150 μm was mechanically milled in liquid nitrogen (cryomilling) to reduce the micron-sized grains in the atomized powders to nanocrystalline size. The milling treatment is similar to that described by Tellkamp *et al.*[9] The nanograined cryomilled particulates were subsequently hot isostatic pressed (hipped) and extruded at 473 K to produce the bulk UFG 5083 Al alloy. The details of the process are given in Figure 1.

Chemical analysis of this material is detailed in Table I. On the basis of the analysis, it is evident that a small additional amount of Mg and impurities were introduced in the material during processing of 5083 Al, and that the alloy includes nitrides and oxides. In particular, Tellkamp *et al.*[9] reported the presence of Mg_2Si, Al_2O_3, and AlN in the alloy after milling.

C. *Annealing*

Small specimens of approximately 1-cm edge length and 5-mm thickness were sectioned from the consolidated extruded billets. These specimens were heated at six different temperatures between 473 and 673 K for different annealing times ranging from 1 to 50 hours. The specimens were quenched in cold water to retain their microstructure after the annealing time periods.

D. *Characterization*

Characterization and grain size measurements were conducted at 10 kV using a PHILIPS*/FEI XL-30 FEG scanning electron microscope (SEM) equipped with an ultrathin window for energy-dispersive spectroscopy. The etchant used to reveal the grain boundaries and microstructure was a solution containing 10 pct H_3PO_4 (85 pct) and 90 pct distilled water. The specimens were dipped into the etchant for 3 to 5 minutes at 323 K and rinsed with methanol.

Samples for transmission electron microscopy were prepared by a combination of mechanical grinding and electrojet polishing. The polishing solution used was of the composition 10 pct HNO_3 and 90 pct Methanol. A current of 20 mA and a voltage of 15 V were used. The temperature of the solution was maintained below 248 K. A FEI/PHILIPS CM 20 transmission electron microscope (TEM) with an accelerating voltage of 200 kV was used for microstructural analysis.

The average grain sizes of the bulk material were measured by using a large number of representative micrographs.

Table I. Chemical Composition of the As-Extruded Bulk UFG 5083 Al Alloy

Elements	Wt Pct
Mg	5.24
Si	0.52
Mn	0.51
N	0.37
O	0.31
Fe	0.25
C	0.164
Zn	0.072
Cu	0.061
Cr	0.017
Ti	0.016
H	0.003
Mo	<0.003
Ni	<0.002
Al	balance

E. *Mechanical Testing*

To study the effect of the annealing treatment at different temperatures on the strength of 5083 Al, the tensile behavior

*PHILIPS is a trademark of Philips Electronic Instruments Corp., Mahwah, NJ.

of the alloy was investigated. Tests were performed in air using (a) a furnace in which the temperature was monitored and maintained constant to within ±2 deg, (b) an initial strain rate of 10^{-3} s^{-1}, and (c) a temperature range of 473 to 673 K.

III. RESULTS

A. *As-Received Microstructure*

Figure 2 shows typical TEM micrographs of the as-extruded UFG 5083 Al alloy. Figure 2(a) provides a low-magnification TEM micrograph showing the duplex distribution of grains in the 5083 Al, some of which are of the order of a few tens of nanometers and others of submicron size. Figure 2(b) shows a typical large grain at high magnification. The presence of irregular extinction contours all along or part of the length of many boundaries and the appearance of poorly delineated transition zones between grains and grain boundaries indicate their nonequilibrium high-energy character. Similar observations have been reported for other UFG alloys.[10–13] Figure 2(c) shows a high-magnification TEM micrograph detailing dislocations in the interior of grains and pinned at the boundaries. The presence of dispersion particles distributed in the interior of grains and pinning dislocations and grain boundaries are also noted.

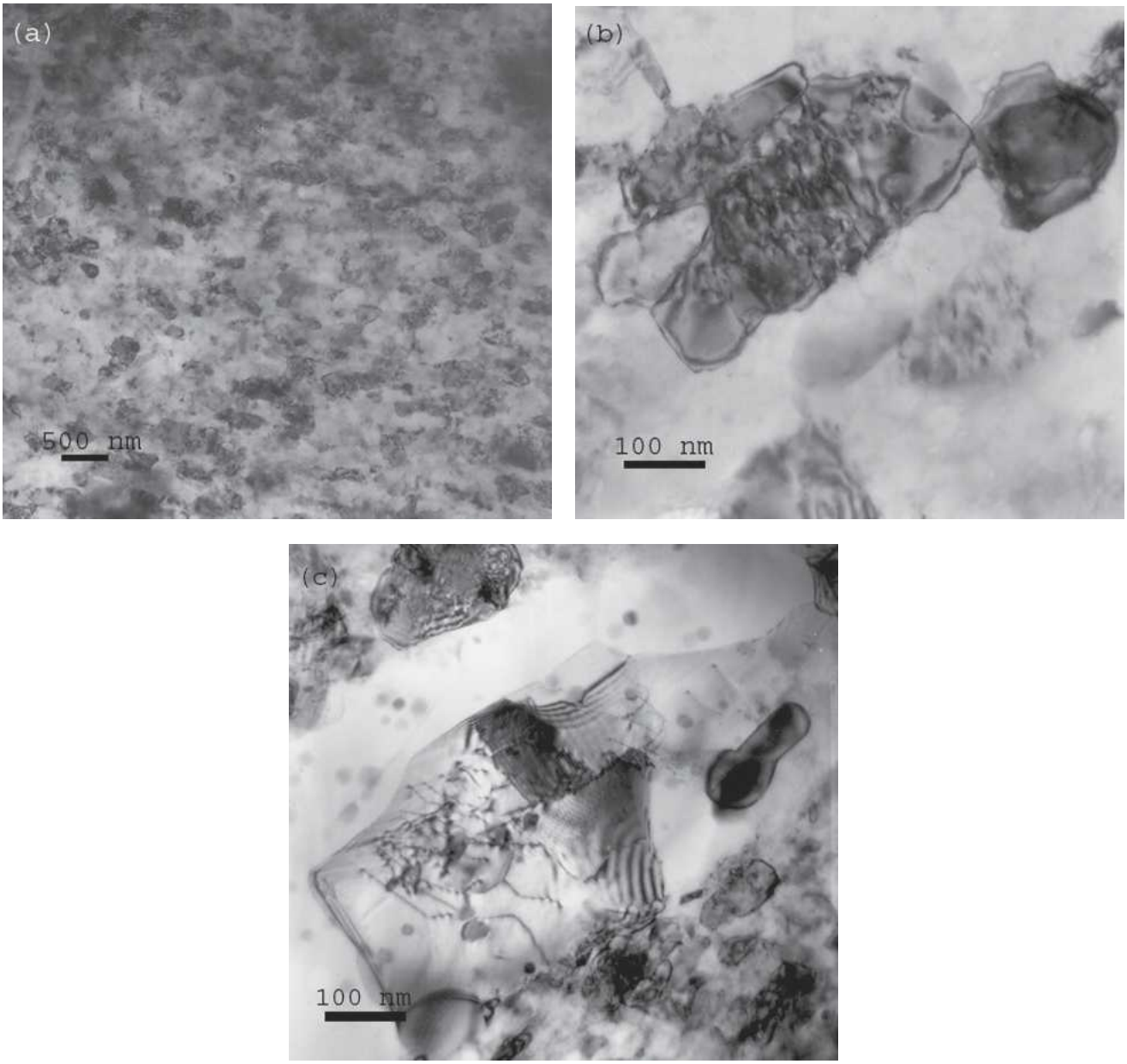

Fig. 2—TEM micrographs of as-extruded UFG 5083 Al. (*a*) Low-magnification showing the duplex distribution of nanocrystalline and ultrafine grains. (*b*) Typical grain at high magnification. Irregular extinction contours and the appearance of poorly delineated transition zones between grains and grain boundaries indicating the high energy unstable character of the microstructure. (*c*) Higher magnification showing dislocations in the grains and arrested at grain boundaries. The presence of a dispersion particle distributed on grains, pinning grain boundaries, and dislocations is observed.

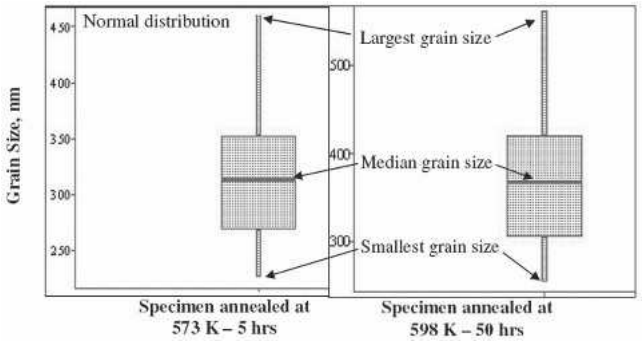

Fig. 3—Box plots showing the spread and skewness of the range of grain size data annealed at 573 and 598 K for 5 and 50 h, respectively.

B. *Grain Growth Behavior*

Statistical analysis was performed on the grain size data to check whether the grain size measurements were representative means of average specimen grain sizes. In Figure 3, grain size data annealed at 573 and 598 K for 5 and 50 hours, respectively, measured from SEM photomicrographs are displayed as a box and whisker plots. The box plot provides a clear picture of the center, the spread, and the skewness of the data distribution and indicates the presence of unusually small (or large) outlying values. The vertical axis represents the measured grain size while the horizontal axis represents the specimens subject to heat treatments at particular temperatures for specific time periods, from which the grain size data were measured. When the box plots were matched with histograms of the same data set, they showed that distribution was normal, and that the measured grain size data fell within 95 pct of the confidence interval, corroborating the validity of the measurements.

The average grain size of the as-extruded material was measured to be ~305 nm. The TEM micrographs were used to check the grain sizes determined from SEM micrographs. The results show that there is good agreement between grain size measured using SEM and that measured using TEM; the maximum difference was about 5 pct. For example, the average initial grain sizes that were measured using SEM and TEM were 305 and 320 nm, respectively.

Figure 4 shows a plot of the average grain size as a function of annealing time. An examination of this figure reveals three observations: (a) the grain size increases with increasing temperature; (b) for a particular temperature, the growth rate decreases with increasing annealing time; and (c) significant grain growth is observed at temperatures higher than 573 K. The latter finding is illustrated in Figures 5(a) and (b), where SEM micrographs show the grain size distribution after annealing at 573 K for 1 hour and 50 hours, respectively. Grain growth is clearly evident in Figure 5(b).

C. *Features of the Annealed Microstructure*

The data show the presence of two regions of behavior, depending on temperature: a low-temperature region ($T <$ 573 K) and a high-temperature region ($T >$ 573 K).

In the low-temperature region that prevails at $T <$ 573 K, limited grain growth occurs. Figure 6(a) provides a representative low-magnification TEM micrograph for a specimen subjected to 50 hours of annealing at 573 K. As shown by the figure, a fair distribution of ultrafine grains with limited grain growth is present. Also, examination of representative

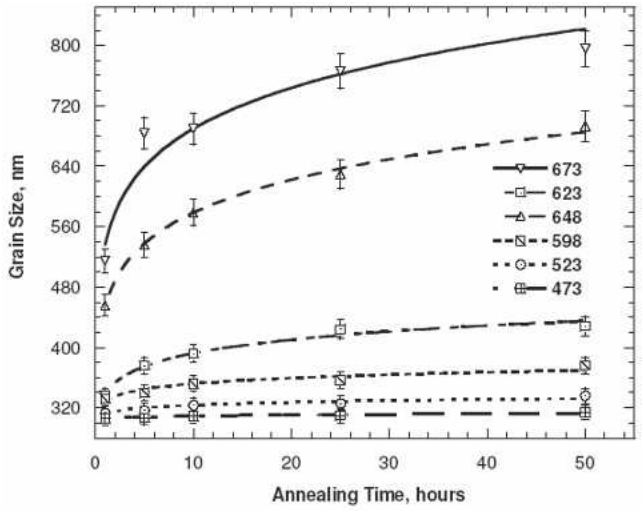

Fig. 4—Instantaneous grain size data as a function of annealing time for different temperatures.

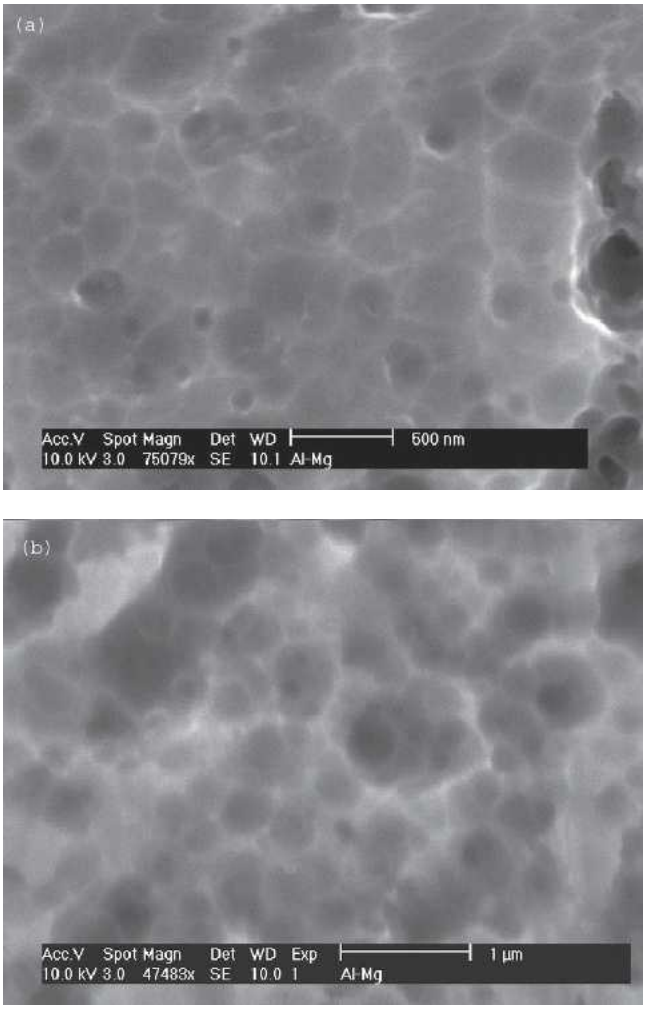

Fig. 5—SEM micrographs showing the grain size distribution after annealing at 573 K: (*a*) 1 h and (*b*) 50 h.

TEM micrographs for specimens annealed in this temperature range (Figure 6(b)) indicates the progress of recovery as reflected in (a) the continuous disappearance of irregular

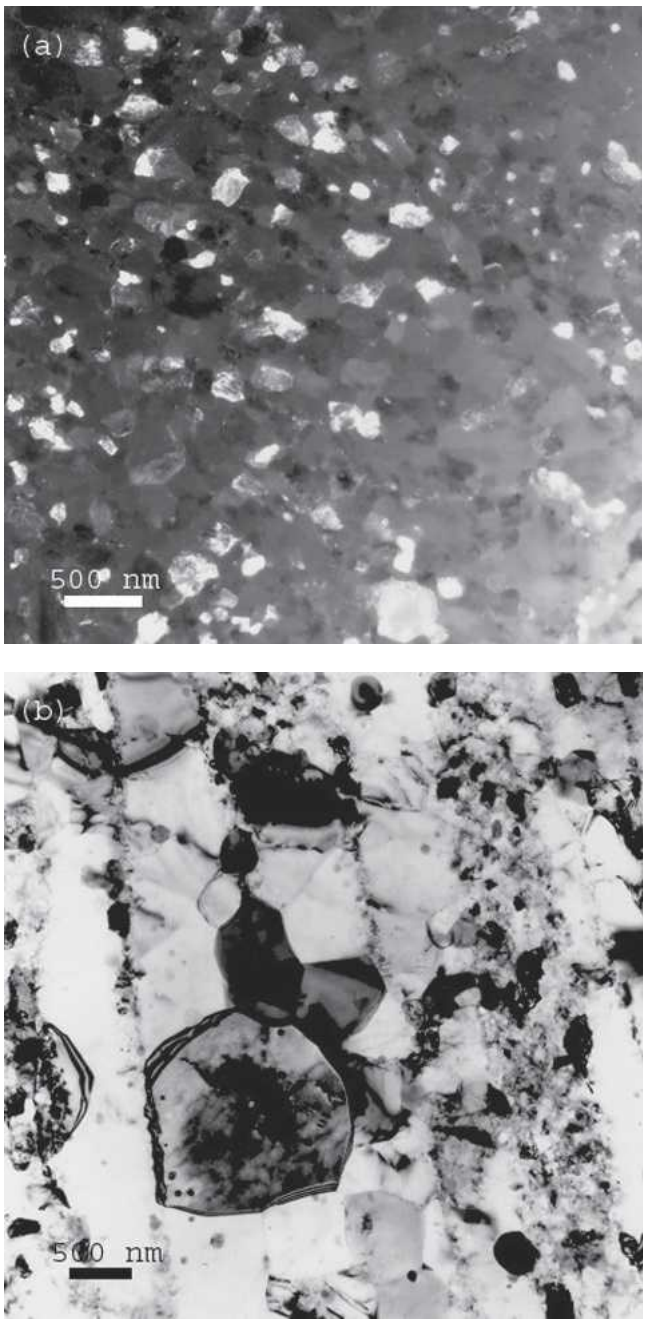

Fig. 6—(*a*) Low-magnification dark-field TEM micrograph of UFG 5083 Al after annealing at 573 K for 50 h showing a fair distribution of ultrafine grains with limited grain growth. (*b*) High-magnification bright-field TEM micrograph showing equiaxed grains, continuous disappearance of irregular contours along grain boundaries, and a gradual decrease in dislocation activity.

contours along grain boundaries and (b) the gradual decrease of dislocation density with increasing temperature.

In the high-temperature region that prevails at $T > 573$ K, the process of recovery seems to be complete and significant grain growth occurs (Figure 7(a)). Figure 7(b) shows the microstructure of postannealed UFG 5083 Al alloy at 623 K for 5 hours. Fewer dislocations than those noted in microstructures characterizing the low-temperature region are seen to be present after annealing. By increasing the time of annealing at 623 K for 50 hours, the TEM micrographs, as exemplified by Figure 7(c), show that annihilation of dislocations seems

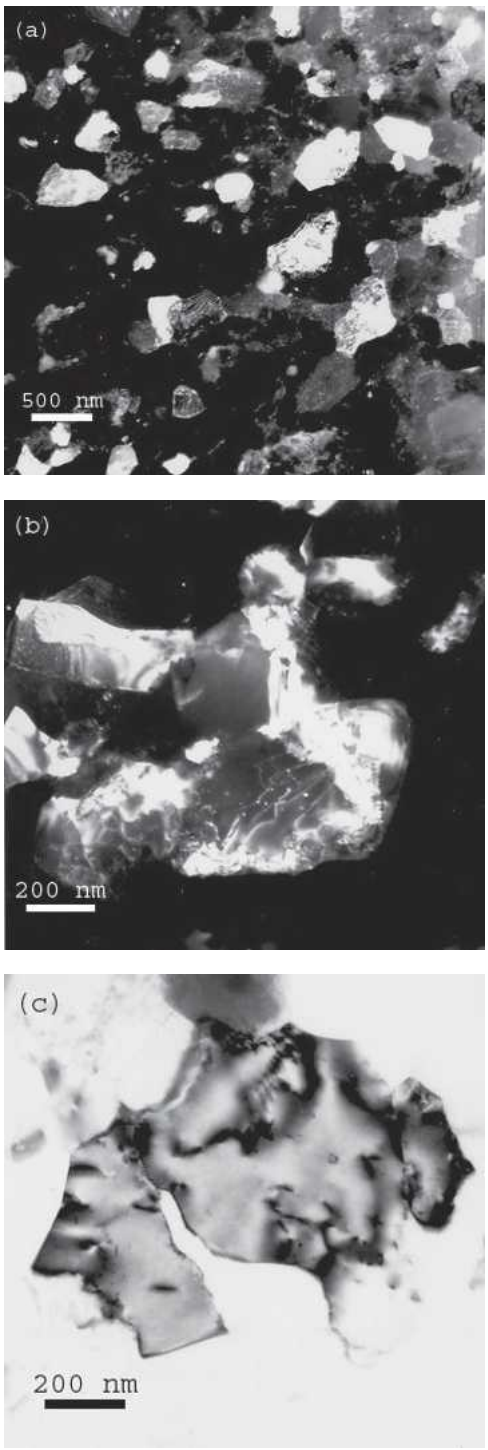

Fig. 7—TEM micrograph of UFG 5083 Al after annealing at (*a*) 623 K for 50 h (low magnification–dark field), (*b*) 623 K for 5 h (dark field), and (*c*) 623 K for 50 h (high magnification–bright field).

to have occurred to a fair extent and that the irregular extinction contours noted along grain boundaries in the TEM micrographs of the as-extruded materials essentially disappear.

D. *Strength as a Function of Annealing Temperature*

Tensile specimens were tested at temperatures in the range of 473 to 673 K at an initial strain rate of 10^{-3} s^{-1}. Figure 8(a) provides an example for the engineering stress–engineering

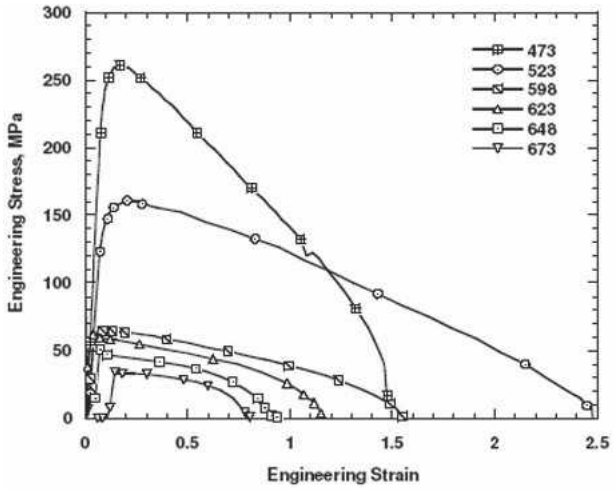

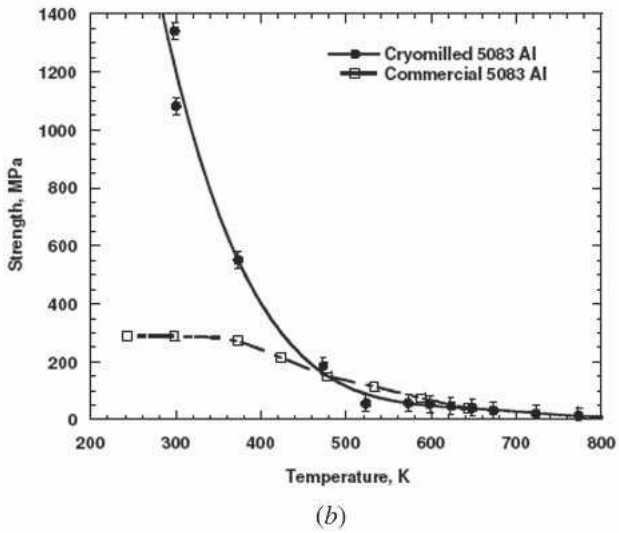

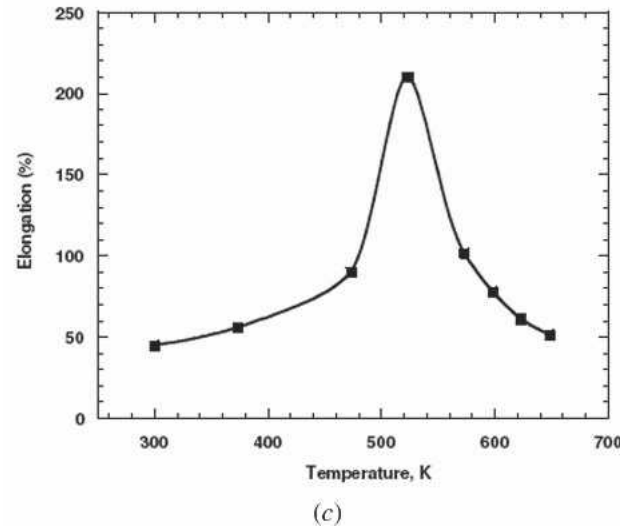

Fig. 8—(*a*) Plot of engineering stress *vs* engineering strain of the alloy tested at 473, 523, 598, 623, and 648 K. (*b*) Plot showing the variation of the ultimate tensile strength as a function of temperature compared to cast commercial 5083-hardened Al alloy.[14] (*c*) Plot of percentage elongation to failure (ductility) as a function of temperature at an initial strain rate of 10^{-3} s^{-1}.

strain curves of the alloy tested at 473, 523, 598, 623, and 648 K. An examination of the figure shows that for each temperature, the engineering stress reaches a maximum value. The data of Figure 8(a) along with those of other temperatures were used to plot the variation of the ultimate strength as a function of temperature in Figure 8(b). An examination of the figure shows that the stress level rapidly decreases with increasing temperature from 473 to 598 K, after which it decreases slowly. For the purpose of comparison, the data on the cast commercial 5083-hardened Al alloy[14] are included. As shown in the figure, the cryomilled 5083 Al is stronger than the cast Al alloy only at temperatures less than 500 K. In addition, inspection of the curves reveals that the decrease in the strength of the cryomilled 5083 Al with temperature is faster than that of the conventional 5083 Al alloy. At temperatures higher than 500 K, the strength of the cryomilled alloy is essentially identical with that of the conventional 5083 Al alloy.

Figure 8(c) shows the percentage elongation to failure (ductility), $\Delta L/L_0$ (pct), where ΔL is the increase in length and L_0 is the initial gage length, as a function of temperature at an initial strain rate of 10^{-3} s^{-1}. The figure shows that a maximum elongation of about 220 pct was achieved at 523 K, and that the elongation decreases at both low temperatures and high temperatures.

IV. DISCUSSION

A. *Grain Growth Kinetics*

The grain growth in conventional polycrystalline materials is normally controlled by atomic diffusion along grain boundaries. The kinetics of this process are frequently represented by the following empirical equation:[15,16,17]

$$D = kt^{1/n} \quad [1]$$

where D is the average instantaneous grain size, t is the annealing time, n is the grain growth exponent, and k is a parameter that depends on temperature but is insensitive to the grain size. The elementary theories of grain growth, which are either based on the proportionality of the growth rate to the interfacial free energy per unit volume[18] or based on the inverse proportionality of the rate of boundary migration to the boundary curvature,[19] predict a value of 2 for n for very pure metals or at very high temperatures. However, experimental data have indicated that in most cases, the value of n is higher than 2, and that for a given metal, it generally decreases with increasing temperature, approaching (in very pure metals or at very high temperatures) the limiting value of 2. For example, n ranged from a value of 20 at low temperatures and decreased to about 3 at higher temperatures for grain growth in nanocrystalline Fe powder.[20] In the Nb-Al nanocrystalline multiphase mixture, Rock *et al.*[21] reported a value of 8 for n.

Equation [1] is not valid during the early stages of growth when the initial grain size D_0 is comparable with D. Under this condition, grain growth can be expressed by the following general form:[16]

$$D^n - D_0^n = kt \quad [2]$$

Equation [2] reduces to Eq. [1] when D_0 is very small compared to D. In addition, by differentiating Eq. [2], the isothermal rate of grain growth can be represented by

$$\frac{dD}{dt} = \frac{k}{n}\left(\frac{1}{D}\right)^{n-1} \quad [3]$$

Equation [3] shows that the rate of grain growth is only related to the instantaneous grain size, D. The data on grain growth in the bulk UFG 5083 Al alloy has been analyzed by using Eq. [3], rather than Eq. [2], because of two reasons. First, Eq. [3] is independent of the initial grain size, D. Second, plotting Eq. [2] in the form of a straight line to deduce the value of n cannot be performed in a straightforward manner.

In order to analyze the experimental data on the basis of Eq. [3], the instantaneous growth rate, dD/dt, was plotted against $1/D$ on a double-logarithmic scale in Figure 9(a). The value of n was estimated from the slope of the straight line, which according to Eq. (3) is equal to $(n - 1)$. The resultant values of the grain growth exponent, n, are plotted against the annealing temperature in Figure 9(b). An examination of this figure shows that the grain growth exponent, n, decreases with annealing temperature, a finding which is consistent with those reported for the grain growth exponent in alloys processed by similar techniques.[20,22,23] For example, according to Figure 9(b), as the temperature increases from 473 to 673 K, the value of n decreases from 23 to 9.4.

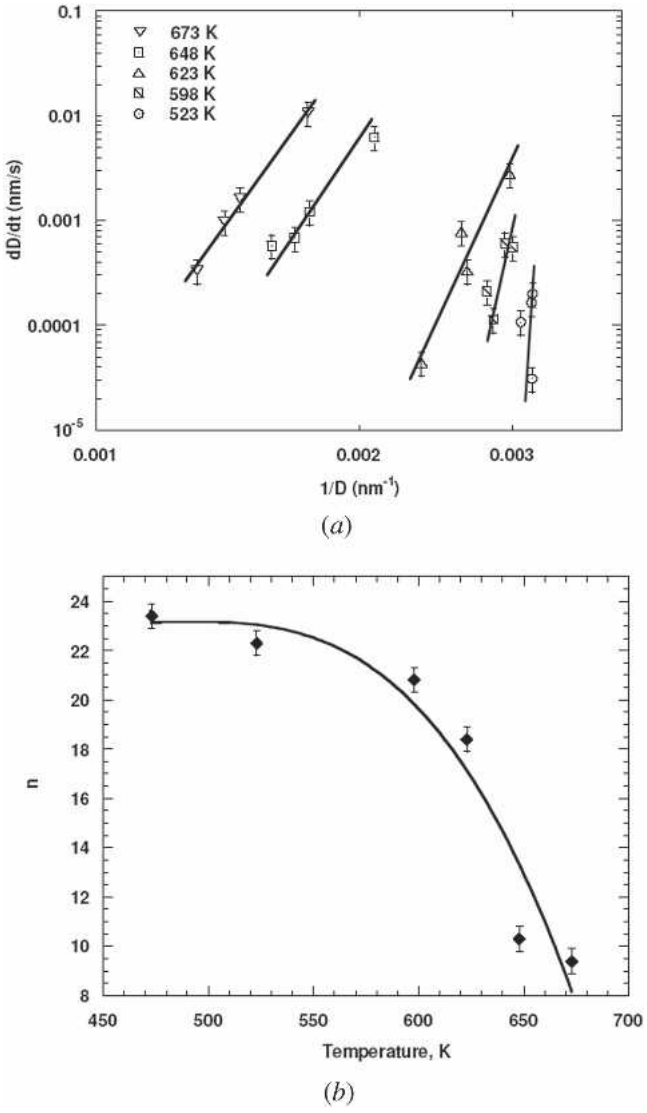

Fig. 9—(*a*) Plot of instantaneous grain growth rate $\frac{dD}{dt}$ as a function of the instantaneous grain size $\frac{1}{D}$ on a double-logarithmic scale. (*b*) Plot of grain growth exponent, n, as a function of annealing temperature.

B. *Activation Energy for Grain Growth*

The activation energy, Q, is often used to determine the microscopic mechanism that dominates the grain growth. The rate constant k in Eq. [2] can be expressed by the Arrhenius equation:

$$k = k_0 \exp\left(\frac{-Q}{RT}\right) \quad [4]$$

where Q is the activation energy for the grain growth, k_0 is a constant that is assumed to be independent of the temperature and time, and R is the molar gas constant.

Zhou *et al.*[24] has reported that the grain growth mechanism in cryomilled powdered Al in low-temperature ranges can be predicted by the theory of grain growth, as represented by Eqs. [2] and [4]. Also, the results of the investigation by Tellkamp *et al.*[9] on grain growth behavior of nanostructured 5083 Al cryomilled powder alloy have demonstrated that the theory of grain growth was applicable and that the grain growth kinetics and activation energy could be determined using Eqs. [3] and [4]. The material selected for the present investigation is the bulk form of the 5083 cryomilled alloy tested by Tellkamp *et al.*[9] Accordingly, it is logical to examine if Eqs. [3] and [4] can predict grain growth in bulk UFG 5083 Al.

By using the values of n and the values of k/n determined from the slopes and the intercepts, respectively, of the straight lines shown in Figure 9(a), the values of k for different annealing temperatures can be determined. In Figure 10, $\ln(k)$ is plotted *vs* $1000/RT$. According to Eq. [3], the slope of the plot gives the value of the activation energy. As indicated by Figure 10, the data fit a curve with negative slopes.

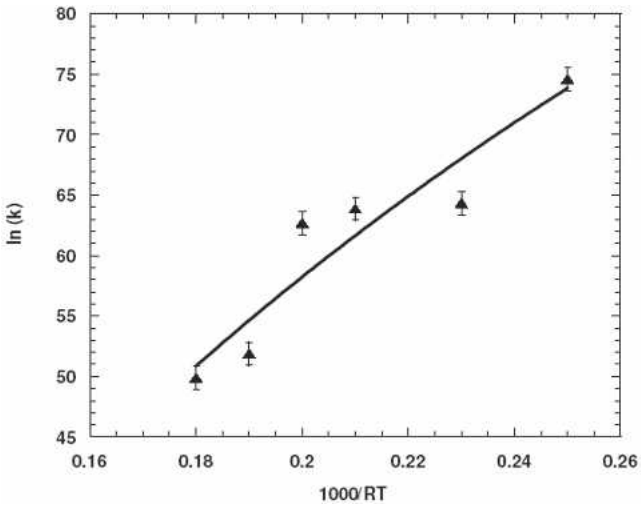

Fig. 10—Plot of ln (*k*) *vs* $\frac{1000}{RT}$ on a linear scale to determine the activation energy of grain growth based on normal grain growth theory.

These negative slopes that signify negative activation energies lead to two conclusions. First, Eqs. [2] through [4], which were found to be applicable to describe grain growth in the cryomilled powder form of 5083 Al alloy, are not valid for the UFG bulk form. Second, other possible mechanisms that may dictate grain growth bulk UFG 5083 Al need to be sought. A possible mechanism along with its rationale is presented herein.

The observation that the grain size exponent, n, inferred from Figure 9(b) is higher than the value of 2 suggests the operation of strong pinning forces on boundaries during the annealing treatment. Consistent with such a suggestion are the details of the microstructure of UFG 5083 Al, as represented by Figures 2(c) and 6(b). These figures show the presence of dispersion particles that are distributed in the grain interior and that some of these particles are seen to pin grain boundaries/dislocations. As discussed earlier, the particles mainly consist of oxides (*e.g.*, Al_2O_3, MgO), carbides (*e.g.*, Al_4C_3), and nitrides (*e.g.*, AlN). These dispersions are incoherent, nanoscale second-phase particles, highly stable at high temperatures, and insoluble in matrix. They act as an effective barrier (dispersion strengthening) to the movement of dislocations and grain boundary migration. The role of these dispersions resembles that of Al_3Sc particles in 5083 Al prepared by ECAP.[25] According to available information, migrating grain boundaries that interact with dispersion particles exert a "toward force" on the particles.[19,26] When sufficient energy is provided, the forces are sufficient to drag the particles through the metal lattice along with the migrating boundaries. Also, during cryomilling, milling media, or atmosphere may result in significant contamination. As a result, interstitial impurities such as O, N, H, C, and solute elements are introduced in the cryomilled material. At elevated service temperatures, they favorably segregate to the grain boundaries, a process that would retard boundary mobility.

As pointed out by Burke,[19] grain growth inhibition by dispersion particles cannot be predicted by traditional kinetic Eqs. [2] and [3]. For that case, he developed a model based on the drag forces exerted by the dispersion particles on the migrating grain boundaries. According to the model, the grain growth rate is not controlled by the instantaneous grain size, D, but rather by the decreasing difference between the ultimate limiting grain size and the changing value of the instantaneous grain size. Burke's model may be expressed by the following equation:

$$\frac{D_0 - D}{D_m} + \ln\left(\frac{D_m - D_0}{D_m - D}\right) = \frac{k_0 t}{D_m^2}\exp\left(\frac{-Q}{RT}\right) \qquad [5]$$

where D_m is the limiting ultimate grain size for the particular annealing temperature. In developing Eq. [5], Burke has assumed that the drag force is independent of grain size. As indicated by Micheles *et al.*,[27] such an assumption is reasonable under the condition that the source of pinning does not depend on grain size. This situation exists when dispersion particles or pores produce pinning. By differentiating Eq. [5], the following basic growth rate equation is obtained:

$$\frac{dD}{dt} = k\left(\frac{1}{D} - \frac{1}{D_m}\right) \qquad [6]$$

Consideration of Eq. [6] indicates that a plot of dD/dt against $1/D$ on a linear scale yields k (slope) and k/D_m (intercept for different temperatures). Such a plot is shown in Figure 11. By combining k and k/D_m, the values of k and D_m for different annealing temperatures can be estimated.

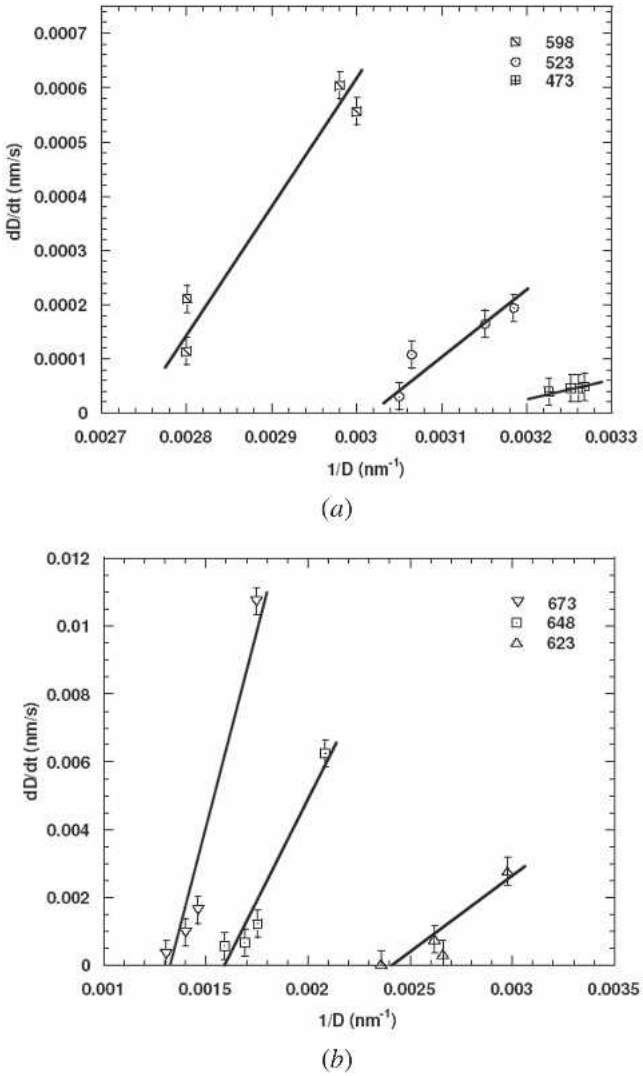

Fig. 11—The plot of $\frac{dD}{dt}$ against $\frac{1}{D}$ on a linear scale yields k (slope) and $\frac{k}{D_m}$ (y intercept) (*a*) for the temperatures 473, 523, and 598 and (*b*) for the temperatures 623, 648, and 673 K.

Having determined the values of k and D_m at various annealing temperatures, attention is now placed on (a) determining whether the concept of grain growth inhibited by particles is characterized by particular activation energies and (b) correlating D_m with the grain growth of the alloy.

1. *Activation energy for grain growth*

For this purpose, ln (k) is plotted *vs* 1000/RT in Figure 12. An inspection of Figure 12 shows the presence of two distinct regions depending on temperature: a high-temperature region with activation energy of 124 ± 5 kJ/mol, and a low-temperature region with activation energy of 25 ± 5 kJ/mol. As demonstrated by the analysis by Micheles *et al.*,[27] the determination of the activation energy for grain growth as determined from the Arrhenius plots (Figure 12) should be independent of whether the pinning force is influenced by grain size.

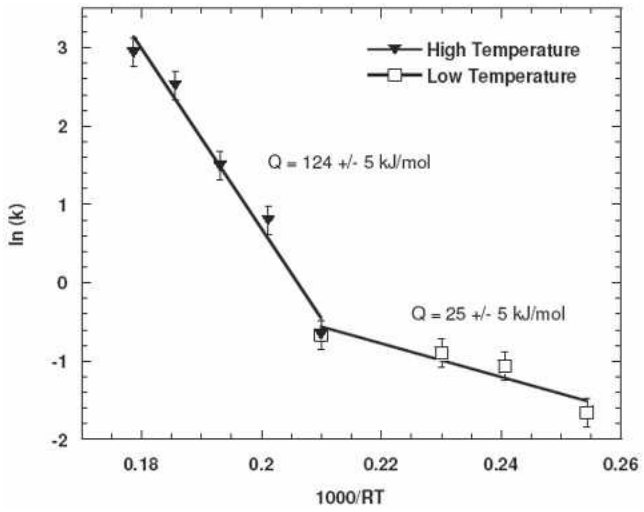

Fig. 12—Plot of ln (k) *vs* $\frac{1000}{RT}$ in high- and low-temperature regimes to determine the activation energy for grain growth when inhibited by dispersion particle drag.

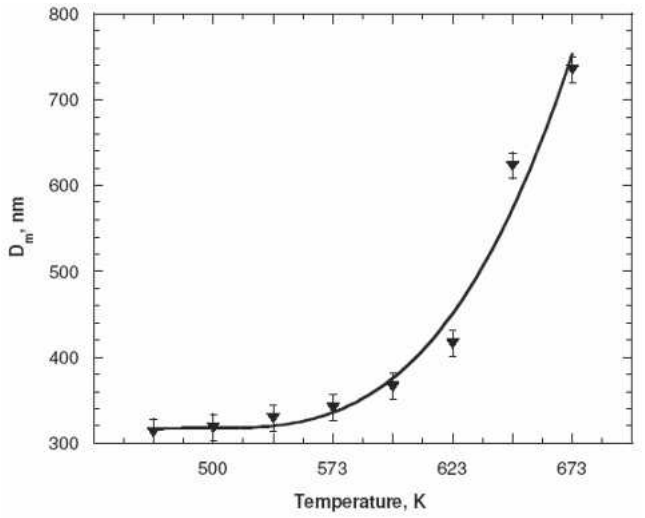

Fig. 13—Plot of maximum grain size attainable, D_m, as a function of annealing temperature.

Several cases having distinctly different activation energies in low- and high-temperature regimes for materials processed by severe plastic deformation or milling were also reported.[9,28,29] For example, Tellkamp *et al*.[9] reported two distinct grain growth regimes: a high-temperature regime (above 654 K) in which $Q \approx 142$ kJ/mol and a low-temperature regime (below 654 K) in which $Q \approx 5.6$ kJ/mol. Also, Rock *et al*.[21] reported a change in the activation energy for grain growth in high- and low-temperature regimes for nanocrystalline Nb-Al multiphase mixture.

At temperatures >573 K, the activation energy is 124 ± 5 kJ/mol. This value falls between the values of grain boundary (86 kJ/mol) and lattice diffusion (143.4 kJ/mol) in polycrystalline aluminum.[30] Zhou *et al*.[22,24] reported the activation energy for the grain growth process inhibited by dispersion particles to be about 112 kJ/mol in processing pure Al by cryomilling. This value is in excellent agreement to the value obtained from the experimental results. In this range of temperatures, the grain structure of UFG 5083 Al alloy attains equilibrium. According to Figure 7, the microstructure at high temperatures has evolved to become fairly large equiaxed grains that are nearly free from strains resulting from cryomilling, consolidation, and extrusion.

At temperatures <573 K, the activation energy is low (25 ± 5 kJ/mol). Also, present substructural data (Figure 6) show that annealing at $T < 573$ K results in limited grain growth. These findings, when combined with the differential scanning calorimetry (DSC) results reported previously at low temperatures on nanostructured Al,[24] nanostructured powder 5083 Al,[9] and a submicrometer-grained Al-3 pct Mg alloy,[29] provide a possible explanation of the low-temperature behavior in terms of the occurrence of a stress relaxation process that results in reordering grain boundaries and reducing the overall strain and energy of the materials without significantly losing the UFG structure. Specifically, it can be suggested that the low activation energy determined in the low-temperature regime is indicative of the highly unstable grain boundaries that need only a small additional driving force to enable rearrangement of grains and grain boundaries. It can also be attributed to the enhanced atomic mobility of the nonequilibrium grain boundaries due to the increased diffusivity arising from the presence of many extrinsic dislocations. As mentioned earlier, 5083 Al powder produced by gas atomization was cryomilled and consolidated to achieve the bulk UFG structure. During cryomilling, considerable strain was induced in the grains. However, as a result of the temperature effect during the hipping and extrusion processes, some stress relaxation takes place in the UF grains. This is consistent with two observations. First, the activation energy of 25 ± 5 kJ/mol obtained in the low-temperature regime is much higher than the cryomilled powder particulates (5.6 kJ/mol) where there is no strain relaxation. Second, the activation energy of 25 ± 5 kJ/mol is slightly lower than that obtained from the equal channel angular pressing (ECAP) of Al-3 pct Mg alloy (30 kJ/mol).

2. *Correlation between* D_m *and mechanical behavior*

The maximum grain size attainable, D_m, is plotted against the annealing temperature in Figure 13. The data define two regions: a low-temperature region and a high-temperature region. The low-temperature region prevails at temperatures lower than 573 K. In this region, D_m changes slowly with annealing temperature and the values of D_m are not greatly different from the initial grain size. On the other hand, the high-temperature region prevails at temperatures higher than 573 K. In this region, the rapid increase in D_m leads to accelerating grain growth.

As shown by Figure 8(b), the ultimate tensile strength of the cryomilled 5083 Al decreases rapidly below 523 K. In this range of temperatures, grain growth is very slow. The continuously rapid decrease in strength with increasing temperature is largely due to the initiation and progress of dynamic recovery that involves annihilation of dislocations, the attainment of equilibrium boundary structure, and the relaxation of stresses induced during cryomilling. When this process approaches the final stage at $T > 523$ K, the strength of the cryomilled 5083 Al becomes essentially similar to that of the cast commercial.

The ductility of the cryomilled 5083 Al exhibits a maximum value of about 220 pct at 523 K. Although research is

in progress to identify the origin of this maximum, one possible explanation that is based on the present data and phenomena associated with high-temperature deformation may be offered. Experimental substructural evidence shows that with increasing temperature from 473 to 523 K, grain growth is limited but the number of equilibrium boundaries increases and dynamic recovery occurs. By contrast, the substructural evidence indicates that at temperatures higher than 523 K, most of the boundaries transform into equilibrium boundaries and grain growth becomes significant with increasing temperature. Combining these two substructural observations with the expected occurrence of boundary sliding due to the ultrafine grain size of the alloy and testing at temperatures higher than 0.5 the melting point (the melting temperature is 853 K) leads to the following possible explanation. By increasing temperature in the range of 473 to 523 K, ductility increases partly because of an increase in the contribution of boundary sliding to deformation as a result of the continuous increase in the number of boundaries at equilibrium along which sliding occurs; and partly because of the annihilation of dislocations and the removal of internal stresses that were introduced by processing. On the other hand, ductility decreases with increasing temperature above 523 K because of a decrease in the contribution of boundary sliding to deformation as a result of the continuous increase in grain size.

CONCLUSIONS

1. The grain growth exponent, n, determined in bulk 5083 Al that was prepared by gas atomization followed by cryomilling, consolidation, and extrusion exhibits a decrease from 23 at 473 K to 9.4 at 673 K.
2. The discrepancy between the present values of n and the value of 2 predicted by elementary theories of grain growth suggests the operation of strong pinning forces on boundaries during the annealing treatment. Consistent with such a suggestion is the initial microstructure of UFG 5083 Al whose details show the presence of dispersion particles that are distributed in the grain interior and that some of these particles are seen to pin grain boundaries/dislocations.
3. Two grain growth regions were identified: a high-temperature region (573 to 673 K) with an activation energy of 124 $\pm$ 5 kJ/mol and a low-temperature region (473 to 573 K) with an activation energy of 25 $\pm$ 5 kJ/mol. The relatively low activation energy (25 $\pm$ 5 kJ/mol) for grain growth in the low-temperature regime is attributed to a stress relaxation process associated with grain boundary readjustment and reordering. The activation energy associated with the high-temperature region (124 $\pm$ 5 kJ/mol) lies between the values reported for grain boundary and lattice diffusion in polycrystalline aluminum systems. In this region, the microstructure evolved to become fairly large equiaxed grains that were nearly free from strains resulting from cryomilling, consolidation, and extrusion. Also, in this region, the controlling mechanism is dispersion particle–inhibited grain growth.
4. As a result of processing 5083 Al by gas atomization followed by cryomilling, fine dispersion particles were introduced. The presence of these dispersion particles provides a contributing factor in the UFG stability in consolidated nanocrystalline materials as compared to materials processed by severe plastic deformation, ECAP, and electrodeposition.
5. The decrease in strength and the presence of maximum ductility with increasing temperature from 473 to 673 K appears to be consistent with substructural changes occurring in the alloy as a result of the annealing treatment.

ACKNOWLEDGMENTS

This work was supported, in part, by the National Science Foundation under Grant No. DMR-0304629 and, in part, by the Marine Corps under Grant No. N00014-03-1-0149. The authors acknowledge the assistance offered by Dr. David Witkin in preparing the material and Dr. W.A. Chiou in using the characterization facility.

REFERENCES

1. H. Gleiter: *Progr. Mater. Sci*., 1989, vol. 33, pp. 223-315.
2. C. Suryanarayana: *Int. Mater. Rev*., 1995, vol. 40, pp. 41-64.
3. H. Gleiter: *Acta Mater*., 2000, vol. 48, pp. 1-29.
4. F.A. Mohamed: *Surf. Interface Anal*., 2001, vol. 31, pp. 532-46.
5. R.J. Perez, H.G. Jiang, and E.J. Lavernia: *Nanostruct. Mater*., 1997, vol. 9, pp. 71-74.
6. H.G. Jiang, M.L. Lau, and E.J. Lavernia: *Nanostruct. Mater*., 1998, vol. 10, pp. 169-78.
7. B. Huang, R.J. Perez, and E.J. Lavernia: *Mater. Sci. Eng*., 1998, vol. A255, pp. 124-32.
8. Z. Lee, R. Rodriguez, R.W. Hayes, E.J. Lavernia, and S.R. Nutt: *Metall. Trans. A*, 2003, vol. 34A, pp. 1473-81.
9. V.L. Tellkamp, S. Dallek, D. Cheng, and E.J. Lavernia: *J. Mater. Res*., 2001, vol. 16, pp. 938-44.
10. R.Z. Abdulov, R.Z. Valiev, and N.A. Krasilnikov: *J. Mater. Sci. Lett*., 1990, vol. 9, pp. 1445-47.
11. R.Z. Valiev, N.A. Krasilnikov, and N.K. Tsenev: *Mater. Sci. Eng*., 1991, vol. A137, pp. 35-40.
12. R.Z. Valiev, F. Chmelik, F. Bordeaux, G. Kapelski, and B. Baudelet: *Scripta Metall. Mater*., 1992, vol. 27, pp. 855-60.
13. R.Z. Valiev, A.V. Korznikov, and R.R. Mulyukov: *Mater. Sci. Eng*., 1993, vol. A168, pp. 141-48.
14. *Metals Handbook*, vol. 2, *Properties and Selection: Nonferrous Alloys and Special Purpose Materials*, ASM International, Materials Park, OH, 1990, p. 93.
15. P.A. Beck, J. Towers, and W.D. Manly: *Trans. TMS-AIME*, 1947, vol. 175, pp. 162-77.
16. P.A. Beck, J.C. Kremer, L.J. Demer, and M.L. Holzworth: *Trans. TMS-AIME*, 1948, vol. 175, pp. 372-400.
17. P.A. Beck: *J. Appl. Phys*., 1948, vol. 19, pp. 507-09.
18. F.A. Mohamed and T.G. Langdon: *Acta Metall*., 1975, vol. 23, pp. 1443-50.
19. J.E. Burke: *Trans. TMS-AIME*, 1949, vol. 180, pp. 73-91.
20. T.R. Malow and C.C. Koch: *Acta Mater*., 1997, vol. 45, pp. 2177-86.
21. C. Rock and K. Okazaki: *Nanostruct. Mater*., 1995, vol. 5, pp. 657-71.
22. F. Zhou, J. Lee, and E.J. Lavernia: *Scripta Mater*., 2001, vol. 44, pp. 2013-17.
23. F. Zhou, X.Z. Liao, Y.T. Zhu, S. Dallek, and E.J. Lavernia: *Acta Mater*., 2003, vol. 51, pp. 2777-91.
24. F. Zhou, J. Lee, S. Dallek, and E.J. Lavernia: *J. Mater. Res*., 2001, vol. 16, pp. 3451-58.
25. D.H. Shin, D.Y. Hwang, Y.J. Oh, and K.T. Park: *Metall. Mater. Trans. A*, 2004, vol. 35A, pp. 825-37.
26. M.F. Ashby and R.M.A. Centamore: *Acta Metall*., 1968, vol. 16, pp. 1081-92.
27. A. Michels, C.E. Krill, H. Ehrhardt, R. Birringer, and D.T. Wu: *Acta Mater*., 1997, vol. 47, pp. 2143-52.
28. J. Wang, M. Furukawa, Z. Horita, M. Nemoto, R.Z. Valiev, and T.G. Langdon: *Mater. Sci. Eng*., 1996, vol. A216, pp. 41-46.
29. J. Wang, Y. Iwahashi, Z. Horita, M. Furukawa, M. Nemoto, R.Z. Valiev, and T.G. Langdon: *Acta Mater*., 1996, vol. 44, pp. 2973-82.
30. F.A. Mohamed and T.G. Langdon: *Metall. Trans*., 1974, vol. 5, pp. 2339-45.